

Chemical Science

Accepted Manuscript

This article can be cited before page numbers have been issued, to do this please use: J. Shum, K. K. Leung, L. Huang, L. C. Lee, M. W. Chiang, M. Yarshova, L. Cheng, Y. PAN, S. Yiu, K. C. Lau, B. Z. Tang and K. K. Lo, *Chem. Sci.*, 2025, DOI: 10.1039/D5SC04772B.



This is an Accepted Manuscript, which has been through the Royal Society of Chemistry peer review process and has been accepted for publication.

Accepted Manuscripts are published online shortly after acceptance, before technical editing, formatting and proof reading. Using this free service, authors can make their results available to the community, in citable form, before we publish the edited article. We will replace this Accepted Manuscript with the edited and formatted Advance Article as soon as it is available.

You can find more information about Accepted Manuscripts in the [Information for Authors](#).

Please note that technical editing may introduce minor changes to the text and/or graphics, which may alter content. The journal's standard [Terms & Conditions](#) and the [Ethical guidelines](#) still apply. In no event shall the Royal Society of Chemistry be held responsible for any errors or omissions in this Accepted Manuscript or any consequences arising from the use of any information it contains.

ARTICLE

Unusual “mesoionic” N⁺S biscyclometallated iridium(III) polypyridine complexes as photosensitisers for photodynamic therapy and type II immunogenic cell death inducersReceived 00th January 20xx,
Accepted 00th January 20xx

DOI: 10.1039/x0xx00000x

Justin Shum,^{ab} Peter Kam-Keung Leung,^{ac} Lili Huang,^a Lawrence Cho-Cheung Lee,^{ab} Maryana Yarshova,^a Lin Cheng,^a Yi Pan,^a Michael Wai-Lun Chiang,^a Ken Shek-Man Yiu,^a Kai-Chung Lau,^a Ben Zhong Tang^{d,e} and Kenneth Kam-Wing Lo^{*ac}

Historically, the classification of mesoionic compounds has been disconcerting, with more confusion arising when these molecules are used as ligands for metal complexes. Many mesoionic compounds are also biologically active and widely used for various therapeutic applications, but mesoionic metal complexes have not seen much prevalence in the field. In this work, we determine the “mesoionic” nature of an unusual and rare series of N⁺S biscyclometallated iridium(III) complexes [Ir(N⁺C)₂(p-ttqt)] (p-ttqt = 1-phenyl-5-thioxo-5,6-dihydro-[1,2,4]triazolo[1,5-c]quinazolin-1-ium-2-thiolate; HN⁺C = 2-phenylpyridine (Hppy) (1), 7,8-benzoquinoline (Hbzq) (2), 2-phenylbenzothiazole (Hbt) (3) and 2-(1-naphthyl)benzothiazole (Hbsn) (4)) as photodynamic therapy (PDT) agents and immunogenic cell death (ICD) inducers. X-ray, infrared spectroscopy and density functional theory studies demonstrate that the mesoionic nature is retained in the iridium(III) complexes. These complexes are ideal PDT agents with no cytotoxicity at micromolar concentrations (IC_{50, dark} > 25 μM), shocking photocytotoxicity at nanomolar concentrations and PI values (IC_{50, light} = 1.5 – 69 nM; PI = 362 – 33,333), and exquisite selectivity toward cancer cells. Furthermore, their localisation in the endoplasmic reticulum (ER) and efficient reactive oxygen species (ROS) generation enable them to act as photoactivated Type II ICD inducers.

Introduction

Mesoionic compounds are structurally defined as a five-membered heterocyclic ring that cannot be satisfactorily represented by any single resonance structure and possesses a dipolar nature with a localised positively charged ring counterbalanced with a negatively charged exocyclic atom. (Scheme 1).¹ The term “mesoionic” has been highly debated, with the most recent calculations highlighting the absence of aromaticity and the exocyclic bond showing more of a double bond character.^{2,3} As an extension, a class of compounds rarely investigated is transition metal complexes with intact mesoionic character. However, these complexes heavily rely on mesoionic synnone as the coordinating ligand, and most work only reports

on their synthesis.⁴ The rarity of mesoionic transition metal complexes and the lack of variation of mesoionic ligands is attributable to their difficult and unknown preparation and purification procedures, instability, ambiguous chelation modes to the metal centre, and the mesoionic properties that are uncertain after coordination. In a therapeutic context, mesoionic compounds are highly bioactive and have been investigated for anti-bacterial, anticancer and anti-inflammatory applications.^{5–10} This popularity has not been extended to mesoionic transition metal complexes due to the aforementioned issues, but research in this frontier area is necessary to elucidate their biological activity and develop new diagnostic and therapeutic tools.

Recently, the synthesis of a new class of fused mesoionic compounds, 1-substituted-5-thioxo-5,6-dihydro-[1,2,4]triazolo[1,5-c]quinazolin-1-ium-2-thiolate (Httqt)¹¹ inspired us to attempt the coordination with an iridium(III) metal centre.

^a Department of Chemistry, City University of Hong Kong, Tat Chee Avenue, Kowloon, Hong Kong, P. R. China. E-mail: bhkenlo@cityu.edu.hk

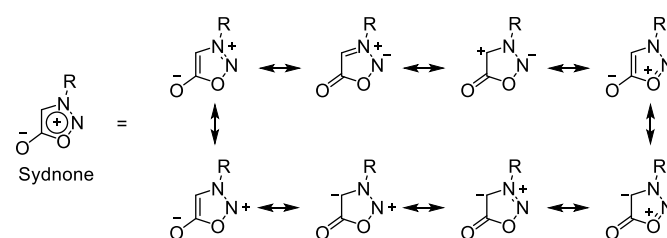
^b Laboratory for Synthetic Chemistry and Chemical Biology Limited, Units 1503-1511, 15/F, Building 17 W, Hong Kong Science Park, New Territories, Hong Kong, P. R. China

^c State Key Laboratory of Terahertz and Millimetre Waves, City University of Hong Kong, Tat Chee Avenue, Kowloon, Hong Kong, P. R. China

^d Department of Chemistry, The Hong Kong University of Science and Technology, Clear Water Bay, Kowloon, Hong Kong, P. R. China

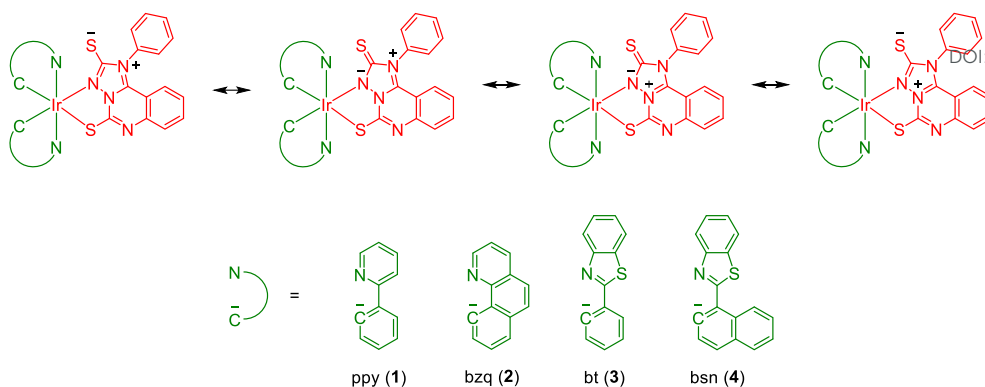
^e School of Science and Engineering, Shenzhen Institute of Aggregate Science and Technology, The Chinese University of Hong Kong, Shenzhen (CUHK-Shenzhen), Shenzhen, Guangdong, 518172 P. R. China

† Electronic supplementary information (ESI) available. See DOI:



Scheme 1 Resonance of synnone as a representative mesoionic compound.



View Article Online
DOI: 10.1039/D5SC04772B**Scheme 2.** Resonance structures of the mesoionic N⁺S⁻ iridium(III) complexes **1** – **4**.

Cyclometallated iridium(III) complexes enable facile attachment of ligands in mild reaction conditions (stirring at room temperature), which is crucial since harsher conditions may affect the stability of the mesoionic ligand. Additionally, cyclometallated iridium(III) complexes are potent photosensitisers for photodynamic therapy (PDT) due to their high biocompatibility, luminescence and reactive oxygen species (ROS) generation.^{12–19} Furthermore, luminescent iridium(III) complexes are shown to be effective immunogenic cell death (ICD) inducers.^{20–23} The demand for PDT agents that can activate Type II ICD response is increasing since these compounds are expected to directly induce endoplasmic reticulum (ER) stress and promote antitumour immunity in a controlled manner.^{24–26}

Herein, we report the synthesis, characterisation and photophysical and photochemical properties of a series of unusual and rare class of neutral mesoionic N⁺S⁻ biscyclometallated iridium(III) complexes [Ir(N⁺C)₂(p-httqt)] (p-httqt = 1-phenyl-5-thioxo-5,6-dihydro-[1,2,4]triazolo[1,5-c]quinazolin-1-ium-2-thiolate; HN⁺C = 2-phenylpyridine (Hppy) (**1**), 7,8-benzoquinoline (Hbzq) (**2**), 2-phenylbenzothiazole (Hbt) (**3**) and 2-(1-naphthyl)benzothiazole (Hbsn) (**4**)) (Scheme 2), and their use as potent photosensitisers and Type II ICD inducers. The structures and “mesoionic” nature of the iridium(III) complexes **1**, **2** and **4** were characterised by X-ray crystallography and density functional theory (DFT) studies. The photophysical properties, electrochemical behaviour and singlet oxygen (¹O₂) generation quantum yields of the complexes, and their photoinduced oxidation of 1,4-dihyronicotinamide adenine dinucleotide (NADH) were examined. Additionally, the aggregation-induced emission (AIE) properties of the complexes were determined. The cellular uptake and cellular localisation of the complexes were also studied by inductively coupled plasma-mass spectrometry (ICP-MS) and laser-scanning confocal microscopy (LSCM), respectively. The (photo)cytotoxicity of the complexes against cancer and normal cells was evaluated by 3-(4,5-dimethylthiazol-2-yl)-2,5-diphenyltetrazolium bromide (MTT) assay. Complex **2** was shown to be the most effective photosensitiser and was used to demonstrate the photoinduced activation of the cell death mechanism and ICD response by using various biological markers.

Results and discussions

Synthesis and characterisation

The ligand p-httqt was synthesised as previously reported.¹¹ The thiourea intermediate was synthesised by condensation reaction with methyl-2-isothiocyanatobenzoate and 4-phenylthiosemicarbazide. Base-catalysed cyclisation of the intermediate thiourea derivative yielded the p-httqt ligand. The ppy (**1**), bzq (**2**), bt (**3**) and bsn (**4**) complexes were prepared from the reaction of the corresponding iridium(III) dimers [Ir₂(N⁺C)₄Cl₂] with p-httqt and Et₃N in CH₂Cl₂/MeOH, purified by column chromatography and recrystallised from CH₂Cl₂/(CH₃)₂CO/Et₂O. All the complexes were characterised by ¹H and ¹³C NMR spectrometry, high-resolution ESI-MS, IR spectroscopy and gave satisfactory elemental analyses. X-ray crystal structures of complexes **1**, **2** and **4** were also investigated. Detailed synthetic procedures and characterisation data are included in the ESI.[†]

Structure and mesoionic elucidation

Biscyclometallated iridium(III) complexes have been reported to coordinate N⁺S⁻ ligands by 3-atom or 4-atom chelation.^{27,28} The presence of multiple nitrogen and sulfur atoms on the httqt ligand could enable facile attachment via N⁺S⁻ chelation to the iridium(III) metal centre, but the coordinating modes can occur in three forms (Fig. 1a). During the purification process of the iridium(III) complexes, we noticed that only one single product was formed. Interestingly, ¹H NMR analyses of the iridium(III) complexes indicated that after coordination, deprotonation of the amine present on the 1,2,4-triazolo[1,5-c]quinazolin-1-ium-2-thiolate ring (Fig. 1b and S1[†]) of the p-httqt ligand occurred and this phenomenon can be observed with the missing broad peak at δ 14.47 in all the complexes (Fig. 1b and S2 – S5[†]). To elucidate the structural form, single crystals of **1**, **2** and **4** were obtained by slow diffusion of Et₂O vapour into a concentrated CH₂Cl₂/(CH₃)₂CO solution of the respective complex. Crystal and structure determination data of the complexes are listed in Tables S1 – S3. Selected bond lengths and angles of **1**, **2** and **4** are listed in Tables S4 – S6, respectively. The perspective drawings of **1**, **2** and **4** are depicted in Fig. S6, 1c and S7,[†]



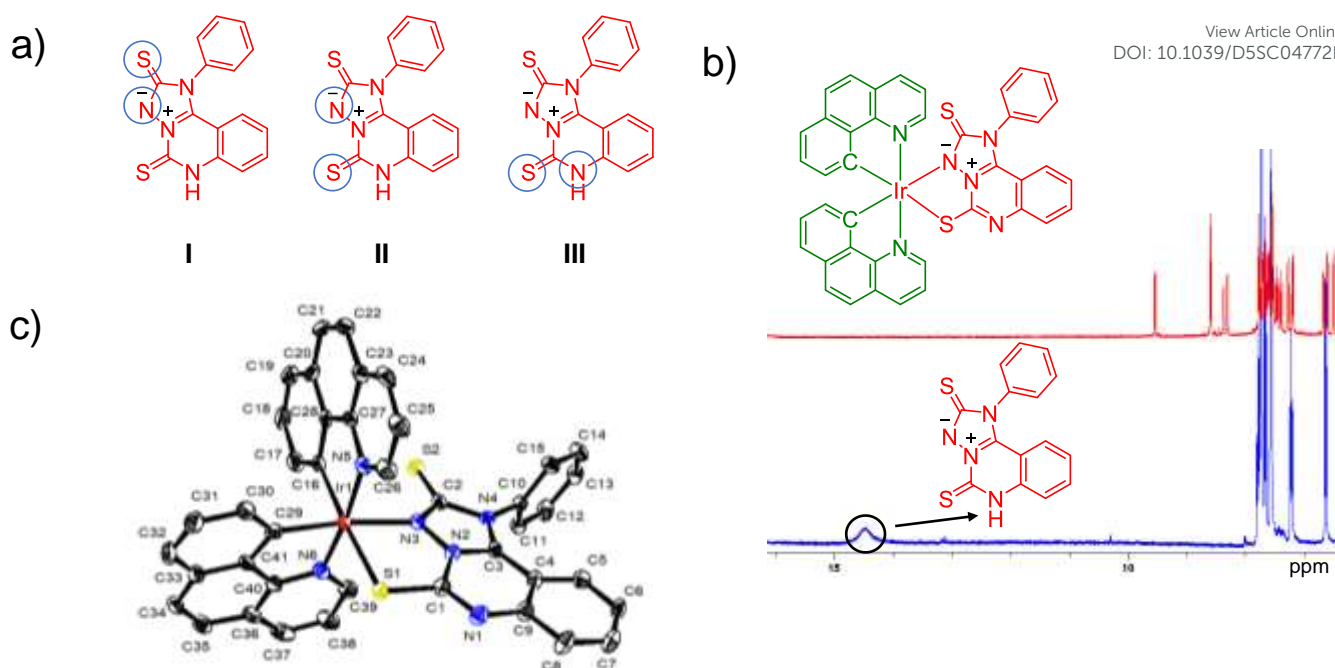


Figure 1. a) Different coordination modes I – III of p-Httqt for N⁺S chelation. b) Magnified ¹H NMR spectra of complex **2** (red) and p-Httqt ligand (blue) in DMSO-*d*₆. c) Perspective drawing of complex **2** with the atomic labelling scheme. Thermal ellipsoids are shown at the 35% probability. Hydrogen atoms are omitted for clarity.

respectively. The structures obtained from X-ray crystallography data demonstrate that the N⁺S iridium(III) complexes preferentially adopt the coordination Form II (Fig. 1a). The iridium(III) centre of **1**, **2** and **4** arrogates a distorted octahedral geometry, and the *trans* angles at the metal centre range from 170.4 to 178.4°, 173.0 to 175.2° and 169.4 to 175.5°, respectively. The Ir–C bonds of the cyclometallated ligands are coordinated to the iridium(III) centre in a *cis* configuration. The *trans*-influence of the carbon donors renders a longer Ir–N bond length in the p-ttqt ligand for **1** (Ir(1)–N(3), 2.171 Å), **2** (Ir(1)–N(3), 2.144 Å) and **4** (Ir(1)–N(3), 2.181 Å) than in their cyclometallating ligands (ppy = Ir(1)–N(5), 2.040 Å; Ir(1)–N(6), 2.070 Å, bzq = Ir(1)–N(5), 2.072 Å; Ir(1)–N(6), 2.042 Å and bsn = Ir(1)–N(5), 2.070 Å; Ir(1)–N(6), 2.056 Å). The bite angles of the cyclometallating ligands (N–Ir–C) and the p-ttqt ligand (N–Ir–S) are close to 80°; similar observations have been made in a related N⁺S biscyclometallated iridium(III) polypyridine system.^{27,29} The phenyl ring and the 1,2,4-triazole ring of the p-ttqt ligand for **1**, **2** and **4** are non-conjugated, and the dihedral angles were determined to be 87.90, 83.97 and 68.60°, respectively, suggestive of a lack of π -conjugation.

In accordance with other reported mesoionic systems,^{2,32} we determined if the iridium(III) complexes are mesoionic based on two factors: 1) double bond character in the exocyclic bond and 2) absence of aromaticity in the 5-membered ring. In complexes **1**, **2** and **4**, the p-ttqt C(2)–S(2) bond lengths are 1.660, 1.647 and 1.650 Å, respectively. These bond length values are noticeably shorter than the average value for compounds with C–S single bonds (1.804 Å),³³ and slightly longer than that of C=S double bonds (1.602 – 1.628 Å).^{34–36} These data suggest that the bonding in these complexes is a combination of resonance structures that feature substantial C=S double bond character. IR spectroscopy measurements also

confirmed the presence of an absorption peak ascribed to a C=S double bond (*ca.* 1320 cm^{–1}). A similar observation has been made in a structurally related compound.³³ The C–N bond lengths of the 1,2,4-triazole ring of complexes **1**, **2** and **4** are in the range of 1.332 Å – 1.430 Å with a significantly longer bond length in the C(2)–N(4) bond (complex **1** = 1.421 Å, complex **2** = 1.415 Å and complex **4** = 1.430 Å). The variation in bond lengths connecting the same atom types (C–N) indicates that the geometric standards for aromaticity are not respected; this agrees with recent calculations of mesoionic azomethine ylides and imines.² Based on the criteria of mesoionic compounds,^{30–32,37} the combined X-ray and IR spectroscopy results of the double bond character of the C(2)–S(2) and lack of aromaticity on the p-ttqt ligand are suggestive of retention of the mesoionic character of the ligand upon coordination to the iridium(III) centre.

To further elucidate the electronic structure and mesoionic nature of the complexes, DFT calculations were performed at the B3LYP-D3(BJ)/def2-SVP and B3LYP-D3(BJ)/def2-TZVP levels using **1** as the model complex. Geometry optimisations of the ground state (*S*₀) were carried out using the polarisable continuum model (PCM) to account for solvation effects in CH₂Cl₂. The optimised bond lengths and bond angles of the *S*₀ structure (Table S7[†]) show excellent agreement with the X-ray crystallographic data, with mean absolute deviations (MADs) of 0.013 – 0.019 Å for selected bond lengths and 1.37 – 2.14° for bond angles. The calculated Wiberg bond indices (Fig. S8[†]) support the absence of aromatic character in the five-membered ring. Specifically, the bond orders are: S(2)–C(2), 1.51; N(4)–C(2), 0.99; N(4)–C(3), 1.20; N(2)–C(3), 1.19; N(2)–N(3), 1.07; and N(3)–C(2), 1.30. These values indicate S(2)–C(2) and N(3)–C(2) bonds possess partial double character, whereas the N(4)–C(2) and N(2)–N(3) are essentially single bonds.



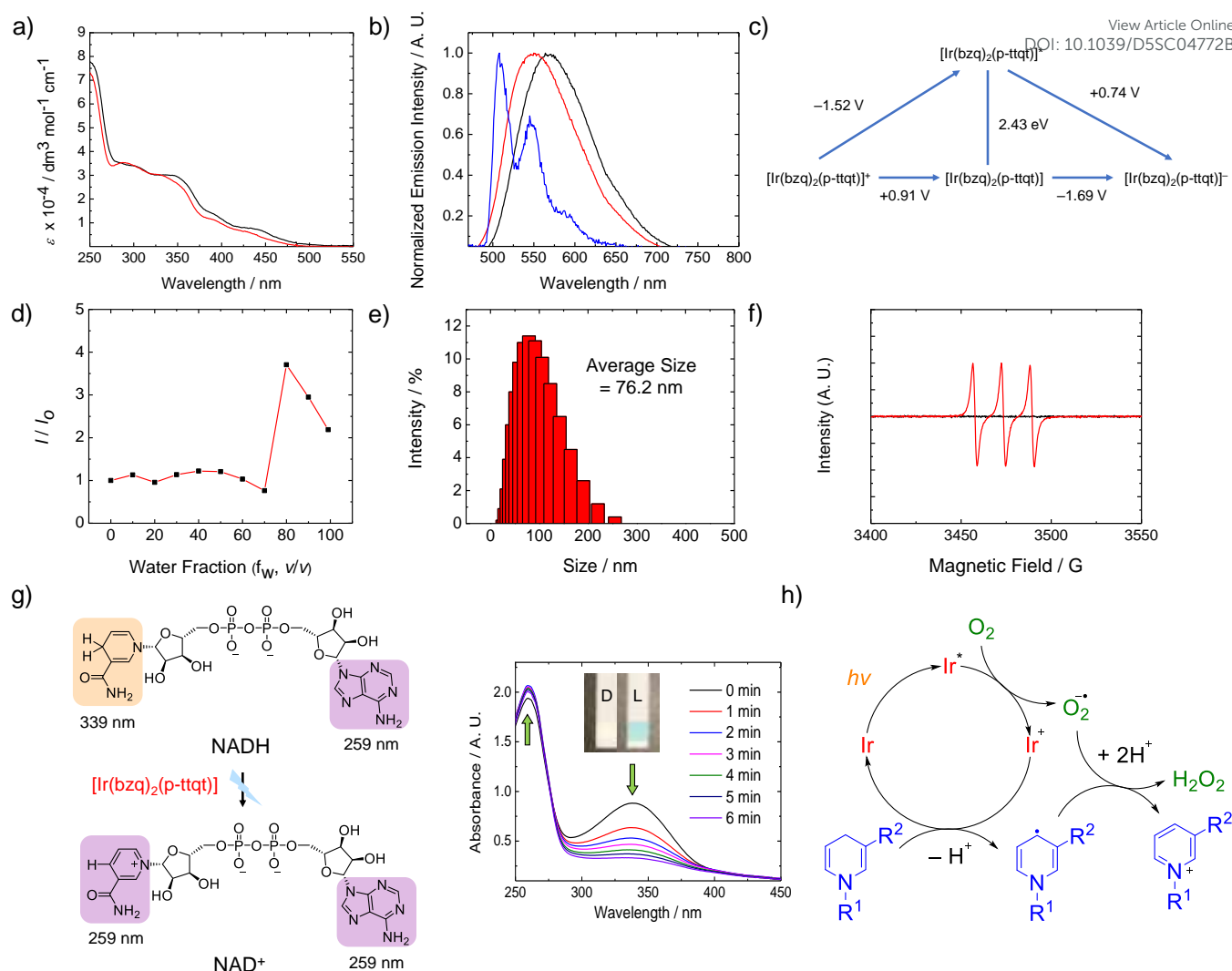


Fig. 2 a) Electronic absorption spectra of complex **2** in CH_2Cl_2 (black) and CH_3CN (red) at 298 K. b) Normalised emission spectra of complex **2** in CH_2Cl_2 (black) and CH_3CN (red) at 298 K and in *n*-butyronitrile at 77 K ($\lambda_{\text{ex}} = 350 \text{ nm}$). c) Latimer diagram showing the ground- and excited-state potentials of complex **2** in CH_3CN at 298 K; potentials are with reference to SCE. d) Relative emission intensities of complex **2** (10 μM) in aerated CH_3CN solutions with various water fractions (f_w , v/v) at 298 K ($\lambda_{\text{ex}} = 350 \text{ nm}$). e) Size distribution of complex **2** (10 μM) in water/DMSO (99:1, v/v). f) ESR signals obtained without (black) and with (red) irradiation at 450 nm (15.5 mW cm^{-2} , 15 min) of aerated CH_3CN solutions containing TEMP (20 mM, $^1\text{O}_2$ scavenger) and complex **2** (10 μM). g) Photooxidation of NADH (100 μM) with complex **2** (10 μM) upon light irradiation (450 nm, 15.5 mW cm^{-2}) at different time intervals in water/DMSO (99:1, v/v). Inset: detection of H_2O_2 after irradiation (D = dark; L = light). h) Proposed photocatalytic cycle for the oxidation of NADH by complexes **1**–**4**.

Photophysical and photochemical properties

The electronic absorption spectral data of the p-Httqt ligand and the complexes are listed in Table S8,[†] and the electronic absorption spectra of the ligand and the complexes are shown in Fig. 2a and S9.[†] All the complexes displayed intense spin-allowed intraligand (^1IL) ($\pi \rightarrow \pi^*$) (N^{AS} and N^{AC}) absorption features in the UV region (*ca.* 250–349 nm, ϵ on the order of $10^4 \text{ dm}^3 \text{ mol}^{-1} \text{ cm}^{-1}$) and weaker spin-allowed metal-to-ligand charge-transfer ($^1\text{MLCT}$) ($d\pi(\text{Ir}) \rightarrow \pi^*(\text{N}^{\text{AS}}$ and $\text{N}^{\text{AC}})$) transitions (*ca.* 350–450 nm). The weaker absorption tailing beyond *ca.* 475 nm is assigned to spin-forbidden $^3\text{MLCT}$ ($d\pi(\text{Ir}) \rightarrow \pi^*(\text{N}^{\text{AS}}$ and $\text{N}^{\text{AC}})$) transitions for complexes **1**–**3**. The spin-forbidden $^3\text{MLCT}$ ($d\pi(\text{Ir}) \rightarrow \pi^*(\text{N}^{\text{AS}}$ and $\text{N}^{\text{AC}})$) transitions for complex **4** are attributed to the weaker absorption tailing beyond *ca.* 490 nm. The assignment of these bands is with reference to previous spectroscopic studies of biscyclometallated iridium(III)

complexes.^{27,38–42} Upon photoexcitation, the complexes exhibited moderately intense and long-lived greenish-yellow to red emission in solutions under ambient conditions and in low-temperature glass. The photophysical data of the ligand and complexes are shown in Table S9,[†] and the emission spectra of the ligand and complexes are presented in Fig. 2b and S10.[†] The ppy (**1**) and bzq (**2**) complexes showed a broad and featureless emission band in fluid solutions at 298 K, indicative of a $^3\text{MLCT}$ ($d\pi(\text{Ir}) \rightarrow \pi^*(\text{N}^{\text{AS}})$)/ $^3\text{ligand-to-ligand charge-transfer}$ (LLCT)($\pi(\text{N}^{\text{AC}}) \rightarrow \pi^*(\text{N}^{\text{AS}})$) emissive state.^{27,38–42} However, complexes **3** and **4** displayed a structured band suggestive of a ^3IL ($\pi \rightarrow \pi^*$)(N^{AC}) emissive state, probably mixed with some $^3\text{MLCT}$ ($d\pi(\text{Ir}) \rightarrow \pi^*(\text{N}^{\text{AC}}/\text{N}^{\text{AS}})$) character. The emission bands of the complexes showed enriched structural features upon cooling the samples to 77 K, attributed to the increased involvement of ^3IL ($\pi \rightarrow \pi^*$) (N^{AS} and N^{AC}) excited-state



character. In general, the emission quantum yields ($\Phi_{\text{em}} > 0.06$) and emission lifetimes ($\tau_0 > 0.24 \mu\text{s}$) of all the complexes are larger than those of previously reported N⁴S biscyclometallated iridium(III) complexes [Ir(N⁴C)₂(N⁴S)].²⁷

Time-dependent DFT (TD-DFT) calculations for complex **1** were subsequently performed to investigate the nature of the low-lying singlet (S₁–S₃) and triplet (T₁–T₄) excited states. The vertical excitation energies of T₁ (2.51 eV) and T₂ (2.55 eV) are nearly degenerate, while T₃ (2.68 eV) and T₄ (2.72 eV) lie at higher energies (Table S10[†]). Inter-fragment charge-transfer (IFCT) analysis (Table S10[†]) was employed to quantify the contributions of MLCT, LMCT, LLCT, IL and metal-centred character in these excitations. The S₀ → T₁ and S₀ → T₂ transitions are primarily ³IL ($\pi(\text{N}^4\text{S}) \rightarrow \pi^*(\text{N}^4\text{S})$), contributing 84.7% and 76.0%, respectively. These are followed by ³MLCT contributions ($d\pi(\text{Ir}) \rightarrow \pi^*(\text{N}^4\text{S})$), 9.1% and 15.3% and, to a lesser extent, ³LLCT ($\pi(\text{ppy}) \rightarrow \pi^*(\text{N}^4\text{S})$), 4.1% and 7.0%, respectively. Natural transition orbital (NTO) analysis of the S₀ → T₁ and S₀ → T₂ excitations also reveals that both the occupied and virtual NTOs are predominantly localised on the N⁴S ligand (Fig. S11[†]).

The electrochemical properties of the p-Httqt ligand and complexes **1** – **4** were investigated by cyclic voltammetry, and their electrochemical data are listed in Table S12.[†] Latimer diagrams were constructed based on their electrochemical data, and the excited-state energy of the complexes was calculated from their emission maxima in low-temperature glass. As indicated in Fig. 2c and S12,[†] the excited-state reduction potential ($E^\circ[\text{Ir}^{+}/^*]$) ranged from –1.06 to –1.52 V versus the saturated calomel electrode (SCE), which are more negative than those of typical ruthenium(II) and iridium(III) complexes,⁴³ highlighting that the complexes are strong photoreductants.

The environment-responsive photophysical properties and ¹O₂ generation capabilities of the complexes are important for developing robust PDT agents. Thus, the complexes were first investigated for their environment-sensitive emission in aerated CH₃CN solutions with various water fractions (f_w , v/v) at 298 K, and their emission responses are illustrated in Fig. 2d and S13.[†] Complexes **1** – **3** displayed enhanced emission intensities upon increasing water fractions; however, this enhancement was reduced upon reaching $f_w = 99\%$. The decrease is attributable to the random agglomeration of amorphous aggregates caused by increased solvent polarity and a decrease in the solubility of the complexes.^{44,45} The increased emission intensities at various water fractions ($f_w = 60 - 90\%$) for complexes **1** – **3** suggested the formation of ordered crystalline nanoaggregates^{44,45} and were confirmed by DLS analysis (Fig. 2e, S14 and S15[†]). At $f_w = 99\%$, a composition suitable for biological applications, complexes **1** and **2**, showed AIE properties that could be useful in enhancing the emission intensity and photocytotoxicity of the complexes. Complex **4**, possessing the most hydrophobic cyclometallating ligand bsn, however, was AIE-inactive with a decreased emission intensity upon increasing water concentrations, even though the complex also underwent aggregation (Fig. S14 and S15[†]).

The ¹O₂ quantum yields (Φ_{Δ}) of the complexes are listed in Table S13,[†] and the Φ_{Δ} values of the complexes in order of highest production are **4** > **1** > **2** > **3**. Complex **4** displayed the largest Φ_{Δ} values which may result from its longest emission lifetime (> 2.00 μs , Table S9[†]). To further confirm the ¹O₂ generation of the complexes, electron spin resonance (ESR) spectroscopy was employed with a ¹O₂ trapper, TEMP. As illustrated in the ESR spectra of the iridium(III) complexes in aerated CH₃CN solutions upon irradiation (Fig. 2f and S16[†]), TEMP is converted to TEMPO after reaction with ¹O₂, leading to an intense 1:1:1 triplet signal. This result indicates that all the iridium(III) complexes can photosensitise ³O₂ to generate ¹O₂.

A crucial coenzyme for redox reactions in living cells is NADH, a useful indicator of the cell's metabolic state.⁴⁶ Induced conversion of intracellular NADH to NAD⁺ in cancer cells can disrupt the redox balance, leading to cell death.^{47–51} The characteristic absorption peaks of NADH ($\lambda = 259$ and 339 nm) and NAD⁺ ($\lambda = 259$ nm) were monitored upon treatment with the complexes and light irradiation (Fig. 2g and S17[†]). All the complexes with light irradiation could induce a significant increase and decrease in absorbance at 259 and 339 nm, respectively, indicative of photoinduced conversion of NADH to NAD⁺. The complete transformation of NADH was observed within 6 min of irradiation time, and the turnover frequency values of the complexes were determined to be 62.7 – 69.4 h^{–1} (Table S14[†]). Interestingly, all the complexes showed reduced or no photoinduced conversion of NADH in degassed solutions (Fig. S18[†]), highlighting the role that oxygen plays in the photocatalytic cycle. The high excited-state reduction potentials of the complexes ($E^\circ[\text{Ir}^{+}/^*] = -1.06$ to -1.52 V versus SCE) are more negative than the reduction potential of oxygen to superoxide anion (*ca.* -0.75 V versus SCE),⁵² indicating that superoxide anion could be formed from oxygen and converted to H₂O₂. Peroxide detection strips (inset of Fig. 2g and S17[†]) confirmed the generation of H₂O₂ and highlighted that the complexes may show similar photocatalytic properties to other previously reported photoreductants.^{53,54} A proposed photocatalytic cycle for the oxidation of NADH by complexes **1** – **4** is shown in Fig. 2h. Notably, the excited-state reduction potentials of the complexes ($E^\circ[\text{Ir}^{+}/^*] = +0.46$ to $+0.74$ V versus SCE) when compared to the reduction potential of NAD⁺ + e[–] + H⁺ → NADH (*ca.* $+0.035$ V versus SCE),⁵⁵ illustrate that the complexes can also feasibly undergo an alternative NADH photooxidation pathway.⁵⁶

Photodynamic therapy efficacy

Based on the promising structural features and chemical properties, the (photo)cytotoxicity of the ligand and complexes **1** – **4** toward cancer (A549 and HeLa) and normal (MRC9) cells was evaluated by the MTT assay (Table 1). The maximum concentration tested for the ligand, complexes **1** – **3** and complex **4** was 100, 50 and 25 μM , respectively, due to solubility reasons. Interestingly, the ligand and complexes were essentially noncytotoxic in cancer and normal cells at their highest soluble concentration (25 – 100 μM) in the dark for 24 h. This noncytotoxic property could be attributed to the chela-



ARTICLE

Table 1. (Photo)cytotoxicity (IC_{50} , μM) of p-Httqt and the iridium(III) complexes **1**–**4** toward cancer and normal cells in the dark and upon irradiation at 450 nm (15.5 mW cm^{-2} , 15 min). PI is the ratio of $IC_{50, \text{dark}}/IC_{50, \text{light}}$.

	A549			HeLa			MRC9		
Compound	$IC_{50, \text{dark}}$	$IC_{50, \text{light}}$	PI	$IC_{50, \text{dark}}$	$IC_{50, \text{light}}$	PI	$IC_{50, \text{dark}}$	$IC_{50, \text{light}}$	PI
p-Httqt	> 100	> 100	— ^a	> 100	> 100	— ^a	> 100	> 100	— ^a
1	> 50	0.027 ± 0.003	> 1,852	> 50	0.015 ± 0.002	> 3,333	> 50	> 50	— ^a
2	> 50	0.0019 ± 0.0001	> 26,316	> 50	0.0015 ± 0.0003	> 33,333	> 50	> 50	— ^a
3	> 50	0.014 ± 0.001	> 3,571	> 50	0.006 ± 0.001	> 8,333	> 50	> 50	— ^a
4	> 25	0.069 ± 0.02	> 362	> 25	0.005 ± 0.001	> 5,000	> 25	> 25	— ^a

^a Could not be determined with accuracy.

tion of the noncytotoxic mesoionic N³S ligand; hence, the coordination of the p-Httqt to the metal centre could bestow low dark cytotoxicity for the resulting metal complex. Surprisingly, upon photoirradiation, the complexes showed no photocytotoxic activity toward normal cells ($IC_{50, \text{light}} > 50 \mu M$ for complexes **1**–**3**; $IC_{50, \text{light}} > 25 \mu M$ for complex **4**). This interesting result is further highlighted by the exceptionally large photocytotoxicity index (PI) values obtained for complexes **1**–**4** (PI = 362 – 33,333) compared to other luminescent biscyclometallated iridium(III) polypyridine complexes.^{57–63}

The cellular localisation of the iridium(III) complexes is important in assessing photoinduced damage since photogenerated ROS have short half-lives and their photocytotoxicity is limited to the surrounding environment. Interestingly, all the complexes showed specific staining of the ER and high Pearson's correlation coefficients ((PCC) = 0.89 – 0.96, Fig. 3a and S19[†]) with ER-Tracker Red in HeLa cells. This result highlights that the complexes may serve as Type II ICD inducers due to their excellent ER localisation and efficient ROS generation. In contrast, the localisation of the complexes in normal MRC9 cells did not show any distinctive staining, and the emission intensity was significantly lower (Fig. S20[†]). The cellular uptake of the iridium(III) complexes in cancer A549 and HeLa and normal MRC9 cells is listed in Table S15.[†] The cellular uptake efficiency of all the complexes is as follows: **2** > **3** > **1** > **4** in both cancer cell lines. All the complexes showed much higher uptake efficiency in cancer cells ($[Ir] = 0.44 - 6.10 \text{ fmol}$) than in normal cells ($[Ir] = 0.07 - 1.01 \text{ fmol}$), which in conjunction with their localisation may account for their low photocytotoxicity toward normal cells (Table 1). Complex **2** displayed almost > 2-fold greater uptake than all the other complexes across both cancer cell lines and could play an important role in its larger photocytotoxic activity. Importantly, all the iridium(III) complexes are potent photosensitisers with exquisite selectivity

toward cancer cells. Complex **2** was used as a model to further study the specific ROS generated intracellularly (Fig. 3b) and the cellular uptake mechanism (Fig. 3c) owing to its high cellular uptake efficiency and large PI values. The photoinduced ROS generated in HeLa cells was characterised by the treatment of ROS inhibitors and ROS indicator CM-H₂DCFDA. Strong fluorescence of the probe was observed upon irradiation of complex **2** alone, indicating the generation of ROS. Pretreatment of HeLa cells with Tiron and NaN₃ ([•]O₂[−] and ¹O₂ scavengers, respectively) led to a sharp decrease in the fluorescence intensity of the ROS indicator. Interestingly, this result indicates that the mesoionic N³S iridium(III) complexes

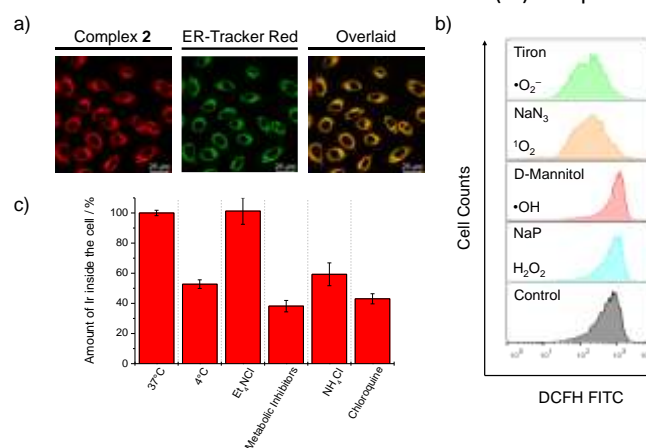


Fig. 3 a) LSCM of HeLa cells treated with complex **2** (10 μM , 24 h, $\lambda_{\text{ex}} = 405 \text{ nm}$, $\lambda_{\text{em}} = 540 - 570 \text{ nm}$) and further incubated with ER-Tracker Red (1 μM , 30 min, $\lambda_{\text{ex}} = 587 \text{ nm}$, $\lambda_{\text{em}} = 610 - 630 \text{ nm}$) (PCC = 0.90). b) Characterisation of specific ROS produced in HeLa cells incubated with complex **2** (500 nM, 24 h) upon irradiation (450 nm, 15.5 mW cm^{-2} , 15 min). Control: No ROS inhibitors. c) Cell uptake mechanism study of complex **2** (10 μM , 1 h) upon pretreatment of different inhibitors/conditions in HeLa cells for 1 h. Control: 37°C, low temperature: 4°C, cation transporter inhibition: Et₄NCl (1 mM), metabolic inhibition: 2-deoxy-D-glucose (50 mM) and oligomycin (5 mM), and endocytic inhibition: NH₄Cl (50 mM) or chloroquine (100 μM).



may activate both Type I and Type II PDT pathways. The cellular uptake mechanism was determined by blocking various pathways via preincubation with different inhibitors in HeLa cells. Upon pretreatment with endocytic or metabolic inhibitors, the internalisation of complex **2** was reduced, suggestive of a primarily energy-dependent endocytosis pathway. This result was further confirmed by preincubation of HeLa cells at 4°C, which also reduced the uptake efficiency of complex **2**.

Cell death mechanism

Cell death mechanisms are often characterised by morphological changes that occur during cell death and can aid or inhibit antitumour response. Complex **2** was used as a model to assess the photoinduced cell death pathway by flow cytometric analysis of HeLa cells stained with annexin V and propidium iodide. As illustrated in Fig. 4a, HeLa cells underwent apoptotic cell death in a dose-dependent manner when treated with complex **2** and light irradiation. Notably, this effect was observed at nanomolar concentrations of complex **2**, with the

apoptotic cells significantly increasing up to 56.2% at $[Ir] = 4.5$ nM. In the absence of light, complex **2** showed a negligible cell mortality rate ($< 3.4\%$), further highlighting the potent photocytotoxic activity and low dark cytotoxicity of the complex.

Apoptotic cell death is characterised by activation of caspases, changes in cell morphology and loss of mitochondrial membrane potential (MMP).^{64–66} Caspases 3 and 7 are a family of inactive proteases but initiate a cascade of downstream signals at the onset of apoptosis. CellEvent™ Caspase-3/7 Red contains a peptide sequence (DEVD) specific to caspase 3/7 conjugated to a fluorogenic nucleus-specific dye and was used to monitor caspase 3/7 activation (Fig. 4b). Untreated and complex **2**-only treated HeLa cells showed no fluorescence, indicating that apoptosis was absent. However, treatment of HeLa cells with complex **2** and light irradiation led to strong fluorescence in the nuclei region, demonstrating that caspase 3/7 was activated and the cells underwent apoptotic cell death. The nuclear morphology of HeLa cells upon treatment with complex **2** without or with light irradiation was assessed by a nuclei-specific dye, Hoechst 33342 (Fig. 4c). In the dark

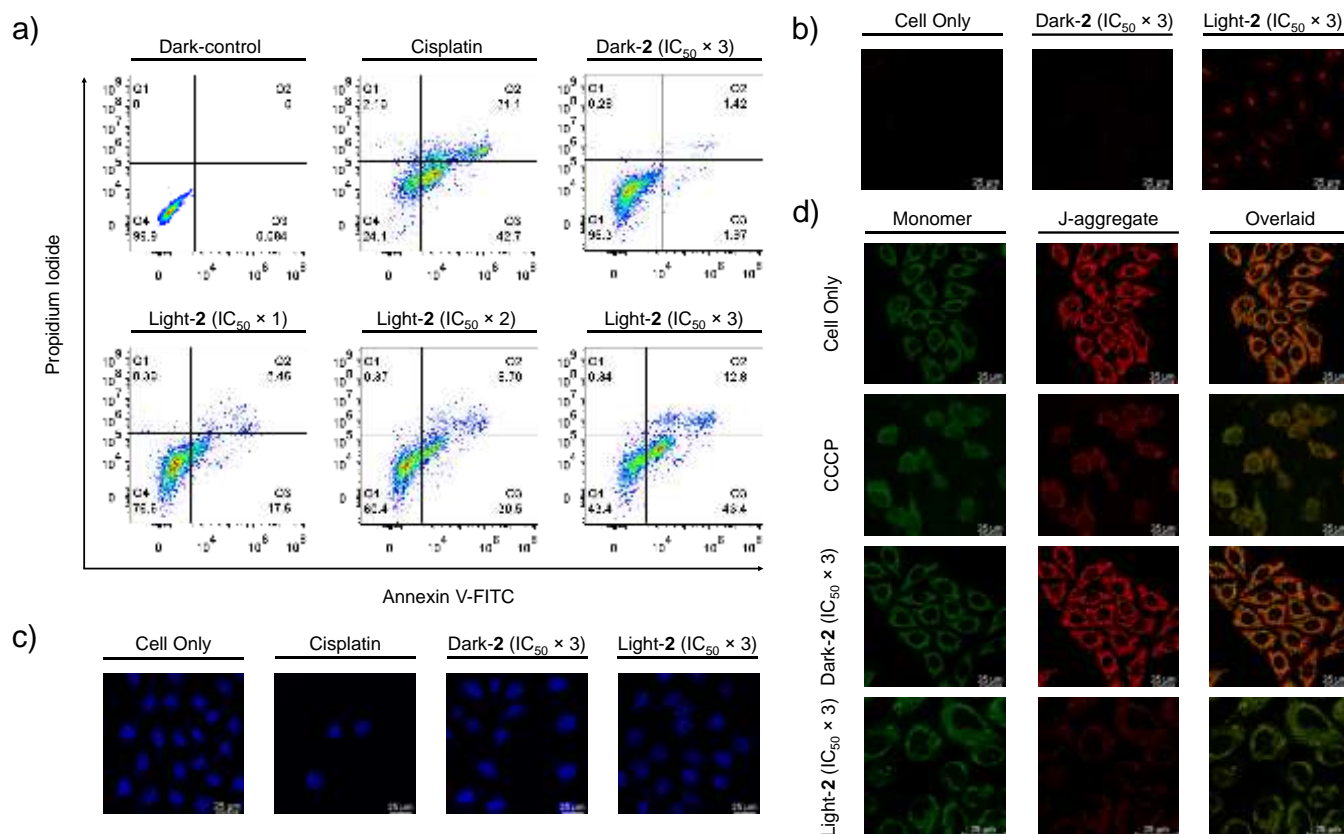


Fig. 4 a) Dot plots of Annexin V-FITC/PI assay on HeLa cells treated with complex **2** (1.5, 3.0 and 4.5 nM) in the dark and with light irradiation. The percentage of cell populations in the respective quadrants is shown as follows: upper left (Q1): necrotic cells, upper right (Q2): late apoptotic cells, bottom right (Q3): early apoptotic cells, and bottom left (Q4): live cells. For dark control, the HeLa cells were untreated. In the positive control, HeLa cells were treated with cisplatin (20 μ M) for 24 h. b) Caspase 3/7 activity of HeLa cells with no treatment or treatment with complex **2** (4.5 nM, 24 h) and further incubated in the dark for 24 h, or treatment with complex **2** (4.5 nM, 24 h), light irradiated, and further incubated for 24 h. All the samples were stained with CellEvent™ Caspase-3/7 Red (20 μ L, 1:100, 1 h, $\lambda_{ex} = 590$ nm, $\lambda_{em} = 610 - 630$ nm). c) Nuclear morphology of HeLa cells with no treatment, treatment with cisplatin (20 μ M, 24 h), treatment with complex **2** (4.5 nM, 24 h) and further incubated in the dark for 24 h, and treatment with complex **2** (4.5 nM, 24 h), light irradiated, and further incubated for 24 h. All the samples were stained with Hoechst 33342 (0.5 μ g/mL, 15 min, $\lambda_{ex} = 405$ nm, $\lambda_{em} = 410 - 430$ nm). d) Mitochondria membrane potential of HeLa cells with no treatment, treatment with CCCP (50 μ M, 15 min) only, or treatment with complex **2** (4.5 nM, 24 h) and further incubated in the dark for 24 h, or treatment with complex **2** (4.5 nM, 24 h), light irradiated, and further incubated for 24 h. All the samples were stained with JC-1 (2 μ g/mL, 20 min, $\lambda_{ex} = 488$ nm, $\lambda_{em, monomer} = 510 - 530$ nm, $\lambda_{em, j-aggregate} = 590 - 610$ nm). In all the experiments, light irradiation = 450 nm, 15.5 mW cm⁻², 15 min.



ARTICLE

condition, treatment of HeLa cells with complex **2** showed a similar nuclear morphology to that of untreated HeLa cells. In contrast, the combined treatment of complex **2** and light irradiation induced nuclear condensation and fragmentation, a common hallmark in apoptosis.

In apoptotic cell death, the loss of MMP triggers the release of signalling proteins that activate apoptotic markers (caspases, cytochrome *c* and apoptosis-inducing factors). The MMP of HeLa cells in response to complex **2** was monitored with JC-1, a mitochondria-specific dye exhibiting green (monomeric) and red (J-aggregate) emission in low and high MMP, respectively (Fig. 4d). HeLa cells that were untreated or incubated with complex **2** only showed similar green and red emission intensities, but treatment with carbonyl cyanide *m*-

chlorophenyl hydrazone (CCCP, an MMP disruptor) would reduce the intensity of the red channel. Similarly, the treatment of HeLa cells with complex **2** and light irradiation significantly disrupted the emission intensity of the J-aggregates, illustrating that the complex can induce loss of MMP upon excitation. Altogether, the nuclear condensation and fragmentation, caspase 3/7 activation and loss of MMP results highlight that the cell death mechanism is based on photoinduced apoptosis.

Induction of immunogenic cell death

The excellent ER-localisation ability and efficient ROS generation of complex **2** can be utilised to develop new Type II

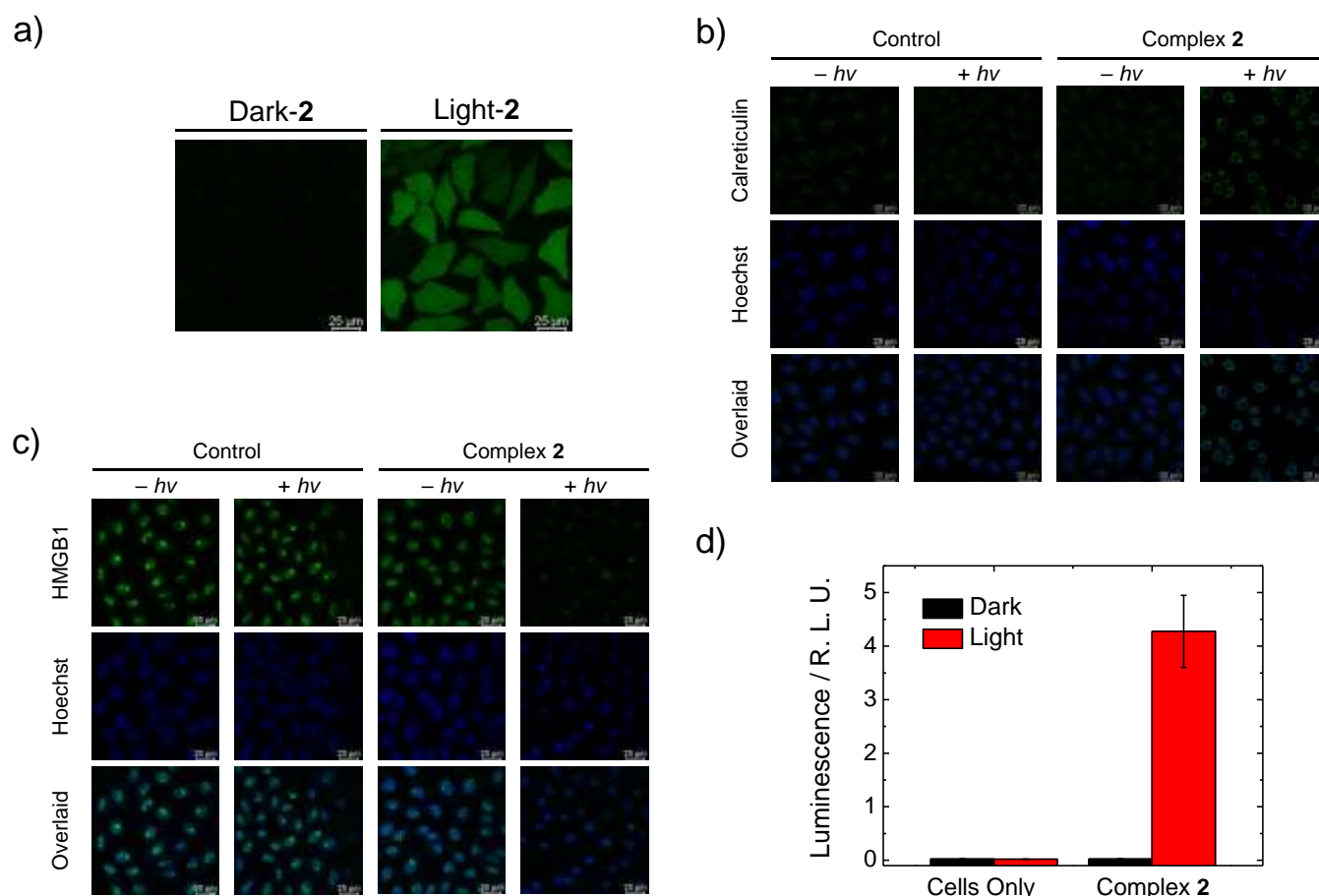


Fig. 5 a) Intracellular calcium content of HeLa cells treated with complex **2** (1 μ M, 24 h) without or with light irradiation, and further incubated with Fluo-4 AM (1 μ M, 30 min, λ_{ex} = 488 nm, λ_{em} = 510 – 530 nm). b) and c) LSCM images of calreticulin or HMGB1 of HeLa cells with no treatment or complex **2** (1 μ M, 24 h), without or with light irradiation. All the samples were incubated with Anti-CALR Polyclonal Antibody (1:200) or Anti-HMGB1 Polyclonal Antibody (1:200) overnight, Alexa Fluor 488-labeled Goat Anti-Rabbit IgG (H + L) (1:500, λ_{ex} = 488 nm, λ_{em} = 510 – 530 nm) for 1 h, and Hoechst 33342 (0.5 μ g/mL, 15 min, λ_{ex} = 405 nm, λ_{em} = 410 – 430 nm) for 15 min with PBS wash (1 mL \times 3) before each subsequent treatment. d) Extracellular ATP levels of HeLa cells treated without or with complex **2** (1 μ M, 24 h) in the dark (black) or with light irradiation (red). In all the experiments, light irradiation = 450 nm, 15.5 mW cm⁻², 15 min.



ARTICLE

ICD inducers. Type II inducers are considered more potent since the generated ROS can directly induce ER stress, a central hub necessary for activating damage-associated molecular patterns (DAMPs) and ICD response. After photoinduced apoptosis by complex **2**, ICD hallmarks like ER stress, exposure of calreticulin on the membrane surface, extracellular release of high mobility group box-1 (HMGB1) and ATP were evaluated in HeLa cells. One function of the ER is calcium homeostasis, and impairment of this role by ROS can induce ER stress that ultimately triggers an inflammatory response.^{67–70} The calcium release from the ER into the cytoplasm after irradiation was determined using Fluo-4 AM, a fluorogenic dye responsive to the spatial dynamics of calcium signalling (Fig. 5a). Incubation of complex **2** with light irradiation resulted in a significant elevation of cytoplasmic calcium concentration compared to the dark condition, suggesting that the ROS generated by complex **2** during photoirradiation can induce ER stress.

Calreticulin, a major DAMP marker, resides in the ER but will translocate during ER stress and early apoptotic phases to the surface of the plasma membrane as an “eat me signal” for recognition by dendritic cells, leading to antitumoural immunity responses.^{67,71} Immunofluorescence imaging showed that no surface expression of calreticulin could be detected in untreated HeLa cells in dark or light conditions, and this observation was similar for HeLa cells only treated with complex **2** in the dark (Fig. 5b). Upon incubation of complex **2** and subsequent irradiation, green immunofluorescence was detected, revealing that surface calreticulin expression was present and could only be induced by the phototherapeutic activity of complex **2**.

Cancer cells undergoing ICD release HMGB1 from the nucleus to the extracellular space due to the permeabilisation of the nuclear lamina and plasma membrane.^{72–74} These extracellular HMGB1 molecules act as DAMPs to regulate inflammation and immune response. As shown in Fig. 5c, strong immunofluorescence staining in the nucleus was detected in untreated HeLa cells without or with irradiation and in HeLa cells treated with complex **2** in the dark. These results illustrate that complex **2** alone cannot translocate HMGB1 to the extracellular space. However, combining complex **2** and light irradiation reduced the emission intensity in the nucleus significantly, indicating that the photoinduced apoptotic effect of complex **2** can enable the release of HMGB1 to the extracellular space.

The secretion of ATP into the extracellular space was determined by a bioluminescence assay. During ICD, the extracellular release of ATP functions as a “find me” signal to enhance tumour recognition of immune cells.^{68,74,75} Notably, only HeLa cells treated with complex **2** and light could induce

the extracellular release of ATP. After photoirradiation, a sharp increase in luminescence was observed (Fig. 5d), corresponding to the extracellular release of ATP. Summing up, from the ER stress, exposure of calreticulin on the membrane surface and extracellular release of HMGB1 and ATP experiments, complex **2** can be identified as a new PDT-based Type II ICD inducer.

Conclusion

We have explored an unusual and rare class of mesoionic N⁴S biscyclometallated iridium(III) complexes and their surprising potency as photosensitisers and photoactivated Type II ICD inducers. Using X-ray crystallography and DFT studies, we demonstrate the retention and elucidation of “mesoionic” character of the complexes after coordination with the p-Httqt ligand. All the complexes are shockingly effective photosensitisers with no cytotoxicity in the dark up to micromolar concentrations ($IC_{50, \text{dark}} > 25 \mu\text{M}$ in cancer A549 and HeLa cells and normal MRC9 cells), extremely high photocytotoxic activity against cancer cells in nanomolar concentrations ($IC_{50, \text{light}} = 0.0019 - 0.069$ and $0.0015 - 0.006 \mu\text{M}$ in A549 and HeLa cell, respectively) with some of the largest PI values ($PI = 362 - 26,316$ and $3,333 - 33,333$ in A549 and HeLa cell, respectively) reported to date for biscyclometallated iridium(III) complexes, and selective photocytotoxicity toward cancer cells. Furthermore, the good ER localisation and 1O_2 generation capabilities of all the iridium(III) complexes enable their use as PDT-activated Type II ICD inducers. Complex **2** displayed the highest photocytotoxic activity and was used as a model to illustrate the uptake pathway, cell death mechanism and the activation of DAMPs during ICD.

Data availability

The data that support the findings of this study are available in the ESI of this article. CCDC 2296948, 2296949 and 2296950 contain the supplementary crystallographic data for this paper. These data can be obtained free of charge via www.ccdc.cam.ac.uk/data_request/cif, or by emailing data_request@ccdc.cam.ac.uk, or by contacting The Cambridge Crystallographic Data Centre, 12 Union Road, Cambridge CB2 1EZ, UK; fax: + 44 1223 336033.

Author contributions

J.S.: conceptualisation, data curation, formal analysis, investigation, writing - original draft, writing - reviewing & editing; P. K.-K. L.: conceptualisation, data curation, formal analysis; L. H.: data curation, formal analysis, writing - reviewing



& editing; L. C.-C. L.: data curation, formal analysis; M. Y.: data curation; L. C.: data curation, formal analysis; Y. P.: data curation, formal analysis; M. W.-L. C.: data curation; K. S.-M. Y.: data curation, formal analysis; K.-C. L.: supervision, writing - review & editing; B. Z. T.: funding acquisition, project administration, supervision, writing - review & editing; K. K.-W. L.: conceptualisation, funding acquisition, project administration, resources, supervision, writing – original draft, writing – review & editing.

Conflicts of interest

There are no conflicts to declare.

Acknowledgements

We thank the Hong Kong Research Grants Council (Project No. CityU 11301121, CityU 11317022, CityU 11309423 and C7075-21GF) and the Hong Kong Research Grants Council and National Natural Science Foundation of China (Project No. N_CityU104/21) for financial support. We also thank the funding support from “Laboratory for Synthetic Chemistry and Chemical Biology” under the Health@InnoHK Programme launched by the Innovation and Technology Commission, The Government of Hong Kong SAR, P. R. China.

References

- W. Baker, W. D. Ollis, *Q. Rev. Chem. Soc.* 1957, **11**, 15.
- P. A. Champagne, K. N. Houk, *J. Org. Chem.* 2017, **82**, 10980.
- S. Wiechmann, T. Freese, M. H. H. Drafz, E. G. Hübner, J. C. Namyslo, M. Nieger, A. Schmidt, *Chem. Commun.* 2014, **50**, 11822.
- X. Bantreil, N. Pétry, F. Lamaty, *Dalton Trans.* 2019, **48**, 15753.
- J. R. Ames, K. T. Potts, M. D. Ryan, P. Kovacic, *Life Sci.* 1986, **39**, 1085.
- D. Liu, J. Zhang, L. Zhao, W. He, Z. Liu, X. Gan, B. Song, *J. Agric. Food Chem.* 2019, **67**, 11860.
- K. Rehse, K.-J. Schleifer, A. Martens, M. Kämpfe, *Arch. Pharm.* 1994, **327**, 393.
- A. W. Brown, T. Holmes, M. Fischer, G. M. Tozer, J. P. A. Harrity, C. Kanthou, *ChemMedChem* 2018, **13**, 2618.
- A. Senff-Ribeiro, A. Echevarria, E. F. Silva, C. R. C. Franco, S. S. Veiga, M. B. M. Oliveira, *Br. J. Cancer* 2004, **91**, 297.
- J. C. Cardoso, S. M. S. C. Cadena, A. Zampronio, A. M. S. Arruda, E. G. S. Carnieri, A. Echevarria, J. Constantin, A. Bracht, M. B. M. Oliveira, *Drug Dev. Res.* 2004, **61**, 207.
- S. M. Kovalenko, O. G. Drushlyak, I. O. Mariutsa, *J. Sulfur Chem.* 2019, **41**, 388.
- X. Zhao, J. Liu, J. Fan, H. Chao, X. Peng, *Chem. Soc. Rev.* 2021, **50**, 4185.
- A. Zamora, G. Viguera, V. Rodríguez, M. D. Santana, J. Ruiz, *Coord. Chem. Rev.* 2018, **360**, 34.
- B. Kar, U. Das, N. Roy, P. Paira, *Coord. Chem. Rev.* 2023, **474**, 214860.
- Y. Wu, S. Li, Y. Chen, W. He, Z. Guo, *Chem. Sci.* 2022, **13**, 5085.
- L. Huang, L. C.-C. Lee, J. Shum, G.-X. Xu, K. K.-W. Lo, *Chem. Commun.* 2024, **60**, 6186.
- L. C.-C. Lee, K. K.-W. Lo, *Chem. Rev.* 2024, **124**, 8825.
- E. C.-L. Mak, Z. Chen, L. C.-C. Lee, P. K.-K. Leung, A. M.-H. Yip, J. Shum, S.-M. Yiu, V. W.-W. Yam, K. K.-W. Lo, *J. Am. Chem. Soc.* 2024, **146**, 25589.
- L. C.-C. Lee, K. K.-W. Lo, *Small Methods*, 2024, **8**, 2400563.
- S. Sen, M. Won, M. S. Levine, Y. Noh, A. C. Sedgwick, J. S. Kim, J. L. Sessler, J. F. Arambula, *Chem. Soc. Rev.* 2022, **51**, 1212.
- K. Xiong, F. Wei, Y. Chen, L. Ji, H. Chao, *Small Methods* 2022, **7**, 2201403.
- Z.-Y. Li, Q.-H. Shen, Z.-W. Mao, C.-P. Tan, *Chem. Asian J.* 2022, **17**, e20220270.
- L. Zhang, N. Montesdeoca, J. Karges, H. Xiao, *Angew. Chem. Int. Ed.* 2023, **62**, e202300662.
- A. P. King, J. J. Wilson, *Chem. Soc. Rev.* 2020, **49**, 8113.
- J.-Y. Zhou, Q.-H. Shen, X.-J. Hong, W.-Y. Zhang, Q. Su, W.-G. Li, B. Cheng, C.-P. Tan, T. Wu, *Chem. Eng. J.* 2023, **474**, 145516.
- L. Wang, R. Guan, L. Xie, X. Liao, K. Xiong, T. W. Rees, Y. Chen, L. Ji, H. Chao, *Angew. Chem. Int. Ed.* 2020, **133**, 4707.
- W.-S. Sie, J.-Y. Jian, T.-C. Su, G.-H. Lee, H. M. Lee, K.-B. Shiu, *J. Organomet. Chem.* 2008, **693**, 1510.
- Y. You, S. Cho, W. Nam, *Inorg. Chem.* 2014, **53**, 1804.
- J. Ruiz, C. Vicente, C. de Haro, D. Bautista, *Inorg. Chem.* 2013, **52**, 974.
- A. M. Simas, J. Miller, P. F. de Athayade Filho, *Can. J. Chem.* 1998, **76**, 869.
- Y. I. Nein, Y. Y. Morzherin, *Russ. Chem. Bull.* 2012, **61**, 1111.
- W. P. Oziminski, C. A. Ramsden, *Tetrahedron* 2015, **71**, 7191.
- D. Sambade, C. Collins, G. Parkin, *J. Mol. Struct.* 2021, **1231**, 129682.
- N. Takeda, N. Tokitoh, R. Okazaki, *Chem. Eur. J.* 1997, **3**, 62.
- A. P. Cox, S. D. Hubbard, H. Kato, *J. Mol. Spectrosc.* 1982, **93**, 196.
- T. Y. Fu, J. R. Scheffer, J. Trotter, *Acta Crystallogr. C Struct. Chem.* 1997, **53**, 1257.
- K. Porte, M. Riomet, C. Figliola, D. Audisio, F. Taran, *Chem. Rev.* 2021, **121**, 6718.
- K. Y. Zhang, H.-W. Liu, M.-C. Tang, A. W.-T. Choi, N. Zhu, X.-G. Wei, K.-C. Lau, K. K.-W. Lo, *Inorg. Chem.* 2015, **54**, 6582.
- K. K.-W. Lo, K. Y. Zhang, C.-K. Chung, K.-Y. Kwok, *Chem. Eur. J.* 2007, **13**, 7110.
- K. K.-W. Lo, J. S.-W. Chan, L.-H. Hui, C.-K. Chung, *Organometallics* 2004, **23**, 3108.
- K. K.-W. Lo, C.-K. Li, J. S.-Y. Lau, *Organometallics* 2005, **24**, 4594.
- L. C.-C. Lee, A. W.-Y. Tsang, H.-W. Liu, K. K.-W. Lo, *Inorg. Chem.* 2020, **59**, 14796.
- C. K. Prier, D. A. Rankic, D. W. C. Macmillan, *Chem. Rev.* 2013, **113**, 5322.
- Y. Dong, J. W.-Y. Lam, A. Qin, J. Sun, J. Liu, Z. Li, J. Sun, H. H.-Y. Sung, I. D. Williams, H. S. Kwok, B. Z. Tang, *Chem. Commun.* 2007, 3255.
- V. Sathish, A. Ramdass, P. Thanasekaran, K.-L. Lu, S. J. Rajagopal, *Photochem. Photobiol. C* 2015, **23**, 25.
- A. Chiarugi, C. Dölle, R. Felici, M. Ziegler, *Nat. Rev. Chem.* 2012, **12**, 741.
- L. Wei, R. Kushwaha, A. Dao, Z. Fan, S. Banerjee, H. Huang, *Chem. Commun.* 2023, **59**, 3083.
- Y. Yang, Y. Gao, J. Zhao, S. Gou, *Inorg. Chem. Front.* 2024, **11**, 436.
- J. Kasparkova, A. Hernández-García, H. Kostrehunova, M. Goicuria, V. Novohradsky, D. Bautista, L. Markova, M. D. Santana, V. Brabec, J. Ruiz, *J. Med. Chem.* 2024, **67**, 691.
- Z. Fan, J. Xie, R. Kushwaha, S. Liang, W. Li, A. A., Mandal, L. Wei, S. Banerjee, H. Huang, *Chem. Asian J.* 2023, **18**, e202300047.
- Z. Fan, Y. Rong, T. Sadhukhan, S. Liang, W. Li, Z. Yuan, Z. Zhu, S. Guo, S. Ji, J. Wang, R. Kushwaha, S. Banerjee, K. Raghavachari, H. Huang, *Angew. Chem. Int. Ed.* 2022, **61**, e202202098.
- D. T. Sawyer, J. L. Jr. Roberts, *J. Electroanal. Chem.* 1966, **12**, 90.



- 53 C. Huang, C. Liang, T. Sadhukhan, S. Banerjee, Z. Fan, T. Li, Z. Zhu, P. Zhang, K. Raghavachari, H. Huang, *Angew. Chem. Int. Ed.* 2021, **60**, 9474.
- 54 Z. Fan, J. Xie, T. Sadhukhan, C. Liang, C. Huang, W. Li, T. Li, P. Zhang, S. Banerjee, K. Raghavachari, H. Huang, *Chem. Eur. J.* 2022, **28**, e202103346.
- 55 Anderson, R. F. *Biochim. Biophys. Acta - Bioenerg.* 1980, **590**, 277.
- 56 H. Huang, S. Banerjee, K. Qiu, P. Zhang, O. Blacque, T. Malcomson, M. J. Paterson, G. J. Clarkson, M. Staniforth, V. G. Stavros, G. Gasser, H. Chao, P. J. Sadler, *Nat. Chem.* 2019, **11**, 1041.
- 57 L. He, C.-P. Tan, R.-R. Ye, M.-H. Chen, J.-J. Cao, L.-N. Ji, Z.-W. Mao, *Chem. Sci.* 2015, **6**, 5409.
- 58 M. Ouyang, L. Zeng, K. Qiu, Y. Chen, L. Ji, H. Chao, *Eur. J. Inorg. Chem.* 2017, **2017**, 1764.
- 59 Y. You, E. J. Cho, H. Kwon, J. Hwang, S. E. Lee, *Chem. Commun.* 2016, **52**, 780.
- 60 P. Zhang, H. Huang, S. Banerjee, G. J. Clarkson, C. Ge, C. Imberti, P. J. Sadler, *Angew. Chem. Int. Ed.* 2018, **58**, 2350.
- 61 L. He, M.-F. Zhang, Z.-Y. Pan, K.-N. Wang, Z.-J. Zhao, Y. Li, Z.-W. Mao, *Chem. Commun.* 2019, **55**, 10472.
- 62 B. Yuan, J. Liu, R. Guan, C. Jin, L. Ji, H. Chao, *Dalton Trans.* 2019, **48**, 6408.
- 63 W.-W. Qin, Z.-Y. Pan, D.-H. Cai, Y. Li, L. He, *Dalton Trans.* **2020**, **49**, 3562.
- 64 J. F. R. Kerr, A. H. Wyllie, A. R. Currie, *Br. J. Cancer* **1972**, **26**, 239.
- 65 R. A. Schwartzman, J. A. Cidlowski, *Endocr. Rev.* **1993**, **14**, 133.
- 66 S. J. Riedl, Y. Shi, *Nat. Rev. Mol. Cell Biol.* **2004**, **5**, 897.
- 67 Y. Xi, L. Chen, J. Tang, B. Yu, W. Shen, X. Niu, *Immunol. Rev.* 2023, **321**, 94.
- 68 D. V. Krysko, A. D. Garg, A. Kaczmarek, O. Krysko, P. Agostinis, P. Vandenabeele, *Nat. Rev. Cancer* 2012, **12**, 860.
- 69 D. Xie, Q. Wang, G. Wu, *Front. Immunol.* 2022, **13**, 1017400.
- 70 J. Fucikova, O. Kepp, L. Kasikova, G. Petroni, T. Yamazaki, P. Liu, L. Zhao, R. Spisek, G. Kroemer, L. Galluzzi, *Cell Death Dis.* 2020, **11**, 1013.
- 71 T. Panaretakis, O. Kepp, U. Brockmeier, A. Tesniere, A.-C. Bjorklund, D. C. Chapman, M. Durchschlag, N. Joza, G. Pierron, P. van Endert, J. Yuan, L. Zitvogel, F. Madeo, D. B. Williams, G. Kroemer, *EMBO J.* 2009, **28**, 578.
- 72 R. Chen, R. Kang, D. Tang, *Exp. Mol. Med.* 2022, **54**, 91.
- 73 M. S. Kwak, H. S. Kim, B. Lee, Y. H. Kim, M. Son, J.-S. Shin, *Front. Immunol.* 2020, **11**, 1189.
- 74 O. Krysko, T. L. Aaes, C. Bachert, P. Vandenabeele, D. V. Krysko, *Cell Death Dis.* 2013, **4**, e631.
- 75 I. Martins, Y. Wang, M. Michaud, Y. Ma, A. Q. Sukkurwala, S. Shen, O. Kepp, D. Métiévier, L. Galluzzi, J.-L. Perfettini, L. Zitvogel, G. Kroemer, *Cell Death Differ.* 2014, **4**, 79.

View Article Online
DOI: 10.1039/D5SC04772B



The data that support the findings of this study are available in the ESI of this article. CCDC 2296948, 2296949, and 2296950 contain the supplementary crystallographic data for this paper. These data can be obtained free of charge via www.ccdc.cam.ac.uk/data_request/cif, or by emailing data_request@ccdc.cam.ac.uk, or by contacting The Cambridge Crystallographic Data Centre, 12 Union Road, Cambridge CB2 1EZ, UK; fax: + 44 1223 336033.

